ARTICLE

Influence of Nanoparticle Shapes of Boehmite Alumina on the Thermal Performance of a Straight Microchannel Printed Circuit Heat Exchanger

Élcio Nogueira[*]

Department of Mechanic and Energy, State University of Rio de Janeiro, Brazil

ABSTRACT

The efficiency and irreversibility defined based on the second law of thermodynamics provide a new path for heat exchangers design and make performance analysis more straightforward and elegant. The second law of thermodynamics is applied in a Straight Microchannel Printed Circuit heat exchanger to determine the thermal performance of different shapes of Boehmite Alumina compared to Al_2O_3 aluminum oxide. The various forms of non-spherical Boehmite Alumina are characterized dynamically and thermodynamically through dynamic viscosity and thermal conductivity, using empirical coefficients. The non-spherical shape includes platelet, cylindrical, blades, and bricks forms. Graphical results are presented for thermal efficiency, thermal irreversibility, heat transfer rate, and nanofluid exit temperature. The non-spherical shapes of Boehmite Alumina show different thermal characteristics concerning the spherical shape when there are variations in fluid flow rates and the nanoparticles fraction. Furthermore, it was theoretically demonstrated that non-spherical particles have higher heat transfer rates than spherical particles, emphasizing platelets and cylindrical shapes for the low volume fraction of nanoparticles and bricks and blades for high volume fraction.

1. Introduction

This work aims to theoretically analyze the thermal performance of a Straight Microchannel Printed Circuit heat exchanger when using non-spherical forms of Boehmite Alumina, compared to the Al_2O_3 aluminum oxide. The methodology is based on thermal efficiency and effectiveness. Efficiency, in this case, is a function of a single dimensionless parameter called the fin analogy, which is like the efficiency of a fin constant-area with an insulated tip, and applies to parallel-flow, counter-flow, and crossflow heat exchangers.

A review of the second law of thermodynamics regarding heat and mass transfer was published during the 1980s, where the fundamental mechanisms responsible for entropy generation were analyzed. It demonstrated how to balance the irreversibility of heat transfer versus the irreversibility of fluid flow and how the reduction in

*Corresponding Author:
Élcio Nogueira,
Department of Mechanic and Energy, State University of Rio de Janeiro, Brazil;
Email: elcionogueira@hotmail.com

irreversibility at the component level affects the entire system. Effectiveness, defined based on the second law, provides a new way to design and analyze heat exchangers, as thermal performance is usually measured by the ratio of current heat transfer rate to ideal transfer rate. However, it does not provide information about efficiency and irreversibility, which measure the degree of entropy generation in a physical system [1-3]. Nogueira, E. applies the second thermodynamics law to analyze and design heat exchangers. For example, he uses this new way for studying a shell and tube and shell and helical coil tube heat exchangers [4,5].

Lei Chai and Savvas A. Tassou [6] state that printed circuit heat exchangers (PCHEs) are a promising technology due to their highly compact construction. They enable high heat transfer coefficients, withstand high pressures, and operate over a wide temperature range. They analyze relatively new heat exchangers and projects that are still in development. They argue that PCHEs are well established in the petrochemical industry. However, they say, it takes a lot of effort to increase the attractiveness of a market that includes a vast range of applications. They mention the need to develop empirical correlations better to predict the performance of the heat exchanger in general.

A printed circuit heat exchanger (PCHE) made of thin diffusion bonded metal plates is lightweight, has high structural strength, enables microchannel processing on the metal surface, is easy to produce, has high reliability and economic efficiency. Moreover, there is almost no thermal resistance between the microchannels to achieve excellent thermal performance. Thermal performance tests were performed for a PCHE for Reynolds numbers in 100-850. It was found that the heat transfer rate increased with increasing Reynolds number in all experiments. Furthermore, empirical correlations were obtained for the heat transfer coefficient for PCHE applications in the analyzed Reynolds number range [7].

Salah Almurtaji et al. [8] argue that heat exchangers are essential in everyday applications. For example, they are used in land vehicles, oil refineries, air conditioning, and water heating. Their review presents state of the art in heat exchanger technology and the use of nanofluids in current devices. In addition, they discuss the development of nanofluids and their influence on the thermo-hydraulic performance of heat exchangers and emphasize the important role of nanofluids in the thermal performance of current heat exchangers.

Iman Zahmatkesh et al. [9] indicate a growing number of published articles related to nanofluids in thermal systems, but there is no specific review on the forms of nanoparticles. The study carried out indicates a lack of de-finitive conclusion on how the shape of nanoparticles affects the performance of thermal systems. They report that the platelet-shaped nanoparticle enables the highest heat transfer rate in natural and forced convection. However, the best performance occurs for a lamina-shaped nanoparticle in the mixed convection regime. They conclude that studies are needed to determine the effective contribution of nanoparticle forms to the thermal performance of energy systems.

Mostafa Monfared et al. [10] Study the effects of the shape of nanoparticles on the entropy generation characteristics in a horizontal double tube heat exchanger. Nanofluids examined include cylindrical, brick, blade, platelet, and spherical nanoparticles. The effects produced by the concentrations of nanoparticles and the different forms of nanoparticles on the rates of thermal entropy generation were investigated numerically. Results indicate that nanofluid containing spherical and platelet-shaped nanoparticles represent, respectively, the maximum and minimum thermal generation rates. Furthermore, it was observed that the rate of thermal entropy generation decreases with an increase in the concentration of nanoparticles, except for those with a spherical shape.

Behrouz Raeia and Sayyed Mohsen Peyghambarzadeh [11] experimentally determined the heat transfer coefficient and thermal efficiency of γ-Al_2O_3/water nanofluids in a double-tube heat exchanger. Nanoparticles dispersed in distilled water range from 0.05% to 0.15% volume fractions. Fluid flows, in turbulent flow regime, show variations in the Reynolds number between 18,000 and 40,000. The addition of nanoparticles to the base fluid allowed an increase in heat transfer of up to 16%. The thermal performance factor reaches 1.11 for nanoparticles concentration equal to 0.15 vol.% and Reynolds number equal to 18,000.

Xiao Feng Zhou and L. Gao [12] estimates the effective thermal conductivity in non-spherical solid particle nanofluids through the differential effective medium theory, considering the interfacial thermal resistance between the solid particles and the host liquids. There was a high increase in the effective thermal conductivity of non-spherical nanoparticles, and the increase in interfacial thermal resistance results in appreciable degradation in the rise in thermal conductivity. The theoretical results agree with experimental data on nanofluids and show the non-linear dependence of the effective thermal conductivity with the volume fractions of non-spherical nanoparticles.

Elena V. Timofeeva et al. [13] investigated experimentally and theoretically modeling the thermal conductivity and viscosity in a fluid consisting of equal volumes of ethylene glycol and water analyzed. They note that the increase

in effective thermal conductivity is greatly diminished by interfacial effects proportional to the total surface area of the nanoparticles and that the surface charge of nanoparticles plays a vital role in viscosity. They demonstrate that adjusting the pH of the nanofluid and reducing the viscosity of the nanofluid without significantly affecting the thermal conductivity. The efficiency of nanofluids the ratio between thermal conductivity and viscosity in both laminar and turbulent flow regimes are evaluated.

2. Methodology

The second law of thermodynamics is applied in a Straight Microchannel Printed Circuit heat exchanger to determine the thermal performance of different forms of Boehmite Alumina compared to Al_2O_3 aluminum oxide. The heat exchanger is represented in Figure 1 below [7].

Figure 1. Straight Microchannel Printed Circuit Heat Exchanger [7]

The various forms of non-spherical Boehmite are characterized dynamically and thermodynamically through dynamic viscosity and thermal conductivity, Equations 6 and 9, using empirical coefficients, presented by Mostafa Monfared et al. [8]. Table 1 gives the properties of hot (Water), cold (Ethylene Glycol) fluids, and nanoparticles of Al_2O_3 and spherical Boehmite Alumina. The non-spherical shape of Boehmite includes platelet, cylindrical, blades,

and bricks forms. Table 2 presents the coefficients used to determine the dynamic viscosity and thermal conductivity for different shapes of Boehmite Alumina.

$$Dh_c = \frac{4 Ac_c Lf_c}{As_c} \qquad (1)$$

Dh_c is the hydraulic diameter, $Ac_c = 42.2 \times 10^{-6} \, m^2$ $Lf_c = 137 \times 10^{-3} \, m$, $Lf_c = 137 \times 10^{-3} \, m$ is the length of the cold flow stream, $As_c = 34.716 \times 10^{-3} \, m^2$ is the total cold area of the heat transfer area.

$$Dh_h = Dh_c \qquad (2)$$

$$Lf_h = \frac{Dh_h As_h}{4 Ac_h} \qquad (3)$$

Lf_h is the length of the hot flow stream, $As_h = 26.037 \times 10^{-3} \, m^2$ is the total hot area of heat transfer area.

The properties of the nanofluids are:

$$\rho_{nano} = \rho_{Particle} \phi + (1 - \Phi) \rho_c \qquad (4)$$

$$\mu_{nano} = \frac{\mu_c}{(1 - \phi)^{2.5}} \qquad (5)$$

$$\mu_{nano} = \mu_c (1 + A_1 \phi + A_2 \phi^2) \quad for\ non-spherical\ shape \qquad (6)$$

$$Cp_{nano} = \frac{Cp_{Particle} \rho_{Particle} \phi + (1 - \phi) \rho_C}{\rho_{nano}} \qquad (7)$$

$$k_{nano} = [\frac{[k_{Particle} + 2k_c + 2(k_{Particle} - k_c)(1 - 0.1)^3 \phi]}{[k_{Particle} + 2k_c + 2(k_{Particle} - k_c)(1 - 0.1)^2 \phi]}] k_c \qquad (8)$$

$$k_{nano} = k_c (1 + C_k \phi) \quad for\ non-spherical\ shape \qquad (9)$$

$$v_{nano} = \frac{\mu_{nano}}{\rho_{nano}} \qquad (10)$$

$$\alpha_{nano} = \frac{k_{nano}}{\rho_{nano} Cp_{nano}} \qquad (11)$$

$$Pr_{nano} = \frac{v_{nano}}{\alpha_{nano}} \qquad (12)$$

$$\mu_W = \frac{\mu_{nano} + \mu_h}{2} \qquad (13)$$

μ_w is the assumed value for the fluid viscosity in the channel wall.

Table 1. Hot (Water), cold (Ethylene Glycol 50%) fluids and nanoparticles properties

	ρ kg/m³	k W/ (m K)	Cp J/(kg K)	μ kg/(m s)	ν m/s²	α m/s²	Pr
Hot	994	0.623	4178	0.72×10^{-3}	7.24×10^{-7}	1.5×10^{-7}	4.83
Cold	1067.5	0.3799	3300	3.39×10^{-3}	2.4045×10^{-5}	1.08×10^{-7}	0.02
Al₂O₃	3950	31.92	873.34	-	-	9.25×10^{-6}	-
B Alumina	3050	30	618.3	-	-	1.59×10^{-5}	-

Table 2. Coefficients defined in Equation 6 and Equation 9 for inclusion of nanoparticle shape in dynamic viscosity and thermal conductivity [8]

Type	C_k	A_1	A_2
Platelets	2.61	37.1	612.6
Blades	2.74	14.6	123.3
Cylindrical	3.95	13.5	904.4
Bricks	3.37	1.9	471.4

$$h_{nano} = 0.1706\,6^{0.44}\,\mathrm{Re}_{nano}^{0.324}\,\mathrm{Pr}_{nano}^{1/3}(\frac{\mu_{nano}}{\mu_W})^{0.14}(\frac{k_{nano}}{Dh_c}) \quad (14)$$

$$h_h = 0.1729\,5^{0.44}\,\mathrm{Re}_h^{0.324}\,\mathrm{Pr}_h^{1/3}(\frac{\mu_h}{\mu_W})^{0.14}(\frac{k_h}{Dh_h}) \quad (15)$$

The heat transfer coefficients of both fluids, cold h_{nano} and hot h_h, were obtained by regression fit [7].

$$A_{Med} = \frac{As_h + As_c}{2} \quad (16)$$

The overall heat transfer coefficient is given by:

$$U_O A = \cfrac{1}{\cfrac{1}{h_h As_h} + \cfrac{1}{h_{nano} As_C} + \cfrac{L}{k_{Metal} A_{Med}}} \quad (17)$$

$k_{Metal} = 16.2\,\mathrm{W/(mK)}$ is the thermal conductivity of the heat transfer plate and $L = 0.4 \times 10^{-3}\,\mathrm{m}$ is the gap between the cold and hot channels.

$$\dot{m}_h = \frac{\mathrm{Re}_h\,\mu_h Ac_h}{Dh_h} \quad (18)$$

$$\dot{m}_{nano} = \frac{\mathrm{Re}_{nano}\,\mu_{nano} Ac_c}{Dh_c} \quad (19)$$

$\dot{m}_h$ and $\dot{m}_{nano}$ are the mass flow rates of the hot and cold fluid, respectively.

$$C_h \doteq m'Cp_h \quad (20)$$

$$C_{nano} \doteq m'Cp_{nano} \quad (21)$$

C_h and C_{nano} are the heat capacity of the hot and cold fluid, respectively.

$$C^* = \frac{C_{min}}{C_{max}} \quad (22)$$

Where C_{min} is the minimum between and C_{nano}.

$$NTU = \frac{U_O A}{C_{min}} \quad (23)$$

NTU are the number of thermal units associated with the heat exchanger.

$$Fa = \frac{NTU(1 - C^*)}{2} \quad (24)$$

Fa is the fin analogy for a counter-flow heat exchanger [2,3,14].

$$\eta_T = \frac{\tanh(Fa)}{Fa} \quad (25)$$

η_T is the thermal efficiency.

$$\varepsilon_T = \cfrac{1}{\cfrac{1}{\eta_T NTU} + \cfrac{1 + C^*}{2}} \quad (26)$$

ε_T is the thermal effectiveness.

$$\dot{Q}_{Max} = (Th_i - Tc_i)C_{min} \quad (27)$$

$\dot{Q}_{Max}$ is the theoretically possible maximum of the heat transfer rate for the situation in analysis.

$$\dot{Q} = \cfrac{(Th_i - Tc_i)C_{min}}{\cfrac{1}{\eta_T NTU} + \cfrac{1 + C^*}{2}} \quad (28)$$

$\dot{Q}$ is the actual heat transfer rate.

The outlet temperatures for both fluids, T_{h0} and T_{c0}, are given by:

$$Th_o = Th_i - \frac{Q'}{m'Cp_h} \quad (29)$$

$$Tc_o = Tc_i + \frac{Q'}{m'Cp_{nano}} \quad (30)$$

$$\sigma_T = (\frac{C_h}{C_{min}})\ln(\frac{Th_o}{Th_i}) + (\frac{C_{nano}}{C_{min}})\ln(\frac{Tc_o}{Tc_i}) \quad (31)$$

σ_T is the thermal irreversibility for the heat exchanger.

3. Results and Discussion

Graphical results related to nanofluid properties, emphasizing momentum diffusivity and thermal diffusivity, are shown in Figures 1 to 4. Figures 6 to 10 show results for heat transfer rate and associated quantities for Re_h=800 and Re_c=200, and Figures 11 to 15 for Re_h=800 and Re_c=600. Figures 16 and 17 show the hot fluid exit temperature with Reynolds numbers ranging from 200 to 400 for hot fluid and cold nanofluid.

Figure 1 presents results for dynamic viscosity for a variation of volume fraction between 0 and 15%. The highlighted figure represents the kinematic viscosity, representing the quantity of motion and having quantitative similarity with the dynamic viscosity. The similarity demonstrates that dynamic viscosity is the main factor in determining the momentum, with specific mass (density) influencing only in the order of magnitude. Non-spherical nanoparticles significantly increase the momentum of the nanofluid, with emphasis on platelets, cylindrical, and blades. The spherical nanoparticles, Al_2O_3 aluminum oxide, and Boehmite Alumina present lower values for the momentum for the entire range of volume fraction analyzed and showed similar graphic results, as they have very

identical numerical thermodynamic properties (Table 1).

Figure 2 presents results for thermal conductivity for a variation of volume fraction between 0 and 15%. Non-spherical Cylindrical Boehmite Alumina has a higher thermal conductivity value than spherical nanoparticles, and Non-spherical Platelets and Blades have lower values. On the other hand, non-spherical Bricks have values very close to spherical particles for a high volume fraction of nanoparticles.

Figure 3 represents the thermal diffusivity and has quantitative similarity with the thermal conductivity. Figure 4 presents results for specific heat for a variety of volume fractions between 0 and 15%. The similarity demonstrates that thermal conductivity is the main factor in determining thermal diffusivity, with specific mass (density) and specific heat influencing only in the order of magnitude.

Figure 5 presents results for thermal capacity for cold and hot fluids as a function of the Reynolds number for a volume fraction equal to 0.05. The thermal capacity increases with increasing Reynolds number for all forms of nanoparticles. The highest values are associated with non-spherical platelets and cylindrical nanoparticles and the lowest in the hot fluid. This result obtained for the hot fluid is significant because the maximum heat transfer rate is theoretically possible, is associated with the lowest thermal capacity between the fluids, and serves as a reference for current heat transfer rates. As the thermal capacity represents the amount of energy in the

form of heat absorbed by the medium, by the different temperature, the presented results will reflect on the heat transfer rate between the fluids.

Figure 6 presents results for heat transfer rate as a function of Reynolds number for volume fraction $\Phi=0.15$. For smaller values of Reynolds numbers, the heat transfer rate significantly approaches the maximum possible, preliminarily indicating that, in this case, the efficiency is relatively low and the irreversibility high. However, the inverse is expected for high Reynolds number values, as the current heat transfer rate is relatively low compared to the maximum possible. In the highlighted figure, the heat transfer rate is presented for the upper range of Reynolds number to better note the dispersion between the results related to the nanoparticle shapes.

Figure 7 presents results of heat transfer rate versus volume fraction for the nanoparticles, with $Re_h=800$ and $Re_c=200$ as parameters. For smaller volume fractions of the nanoparticles, it is observed that the platelet and cylindrical particles have a higher heat transfer rate. However, the brick-shaped particles and blade surpass the two previously mentioned heat transfer rates for high volume fraction values. In the entire range of volume fractions analyzed, the lowest values for heat transfer rate are associated with spherical particles.
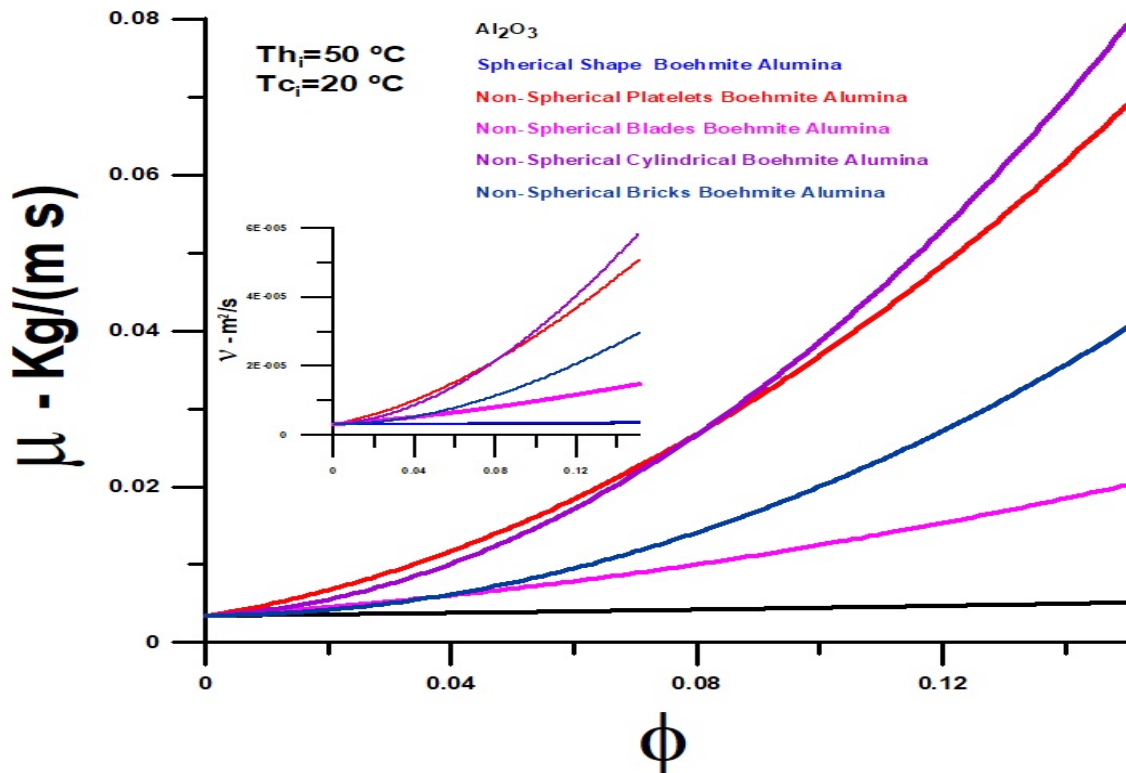

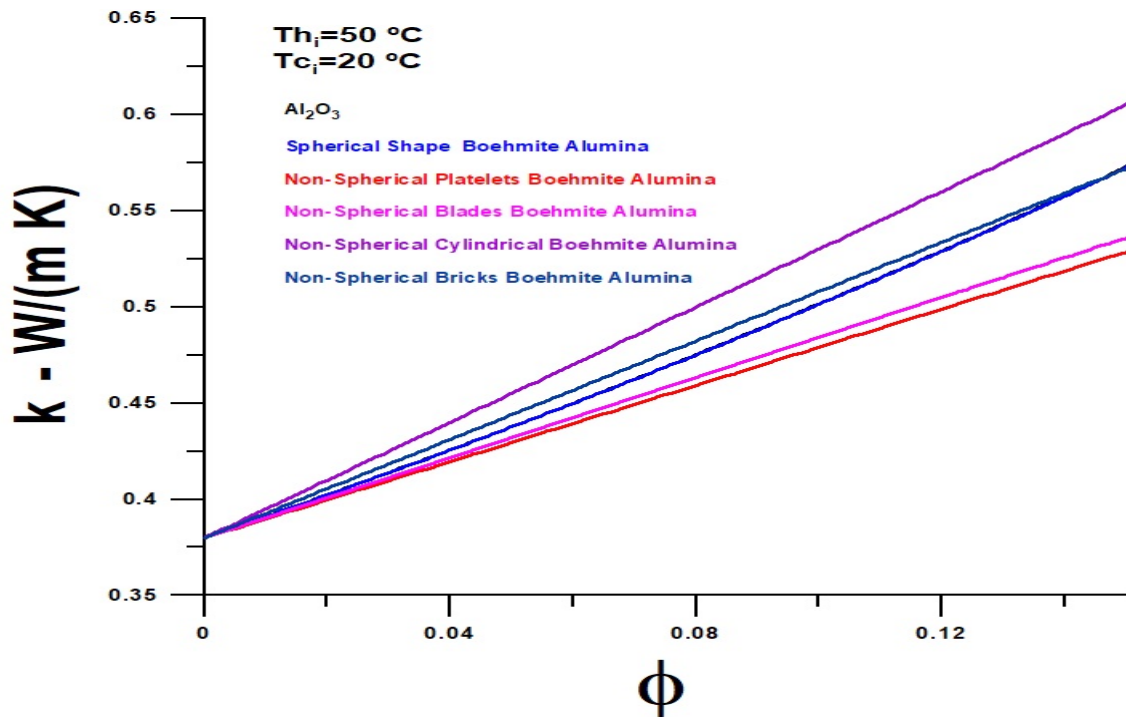**Figure 1.** Dynamic and kinematic viscosities versus nanoparticle volume fraction

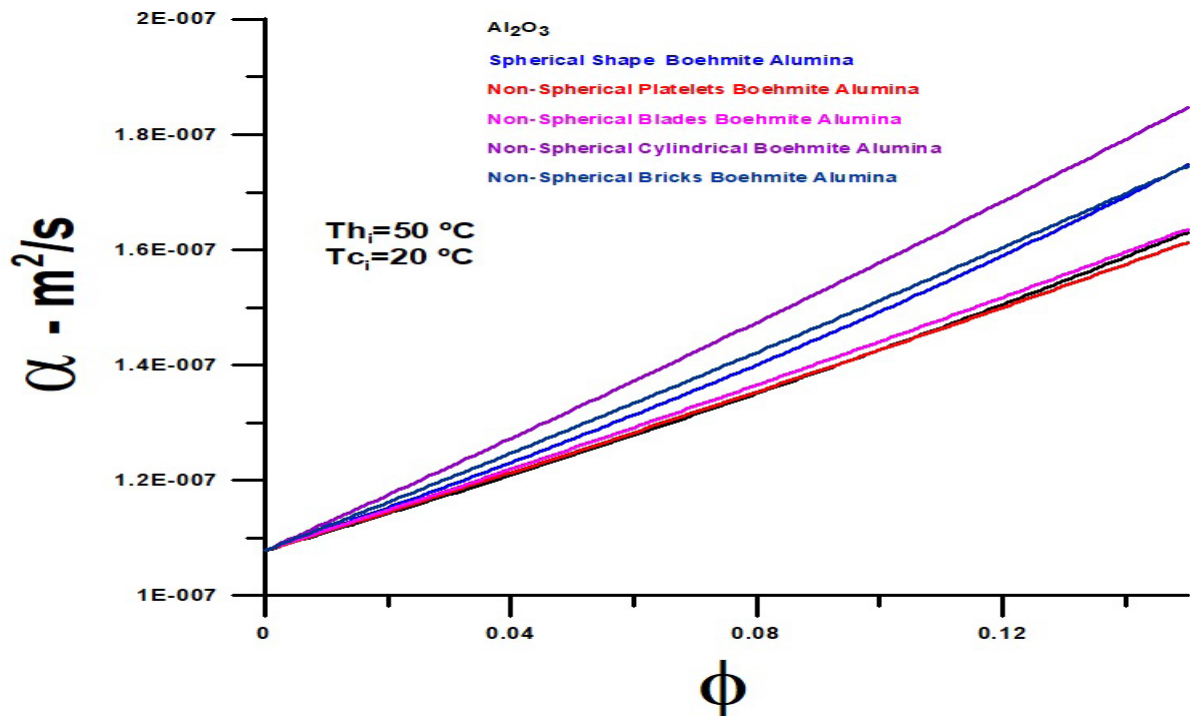**Figure 2.** Thermal conductivity versus nanoparticle volume fraction

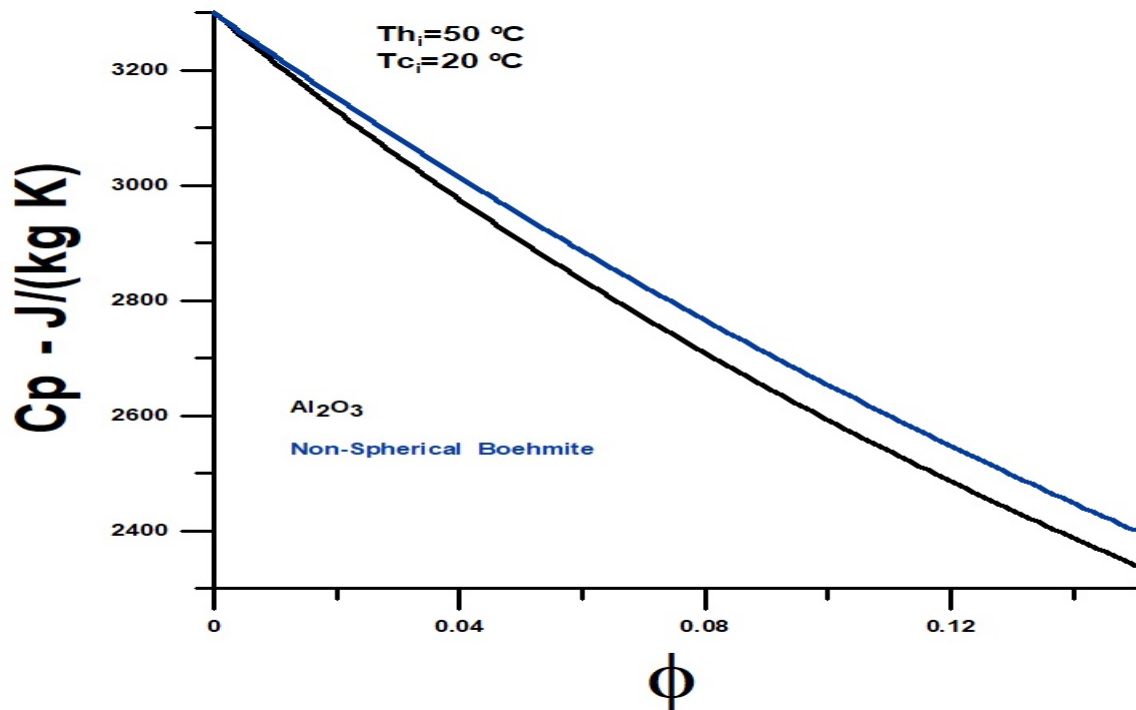**Figure 3.** Thermal diffusivity versus nanoparticle volume fraction

Figure 4. Specific heat and thermal diffusivity versus nanoparticle volume fraction
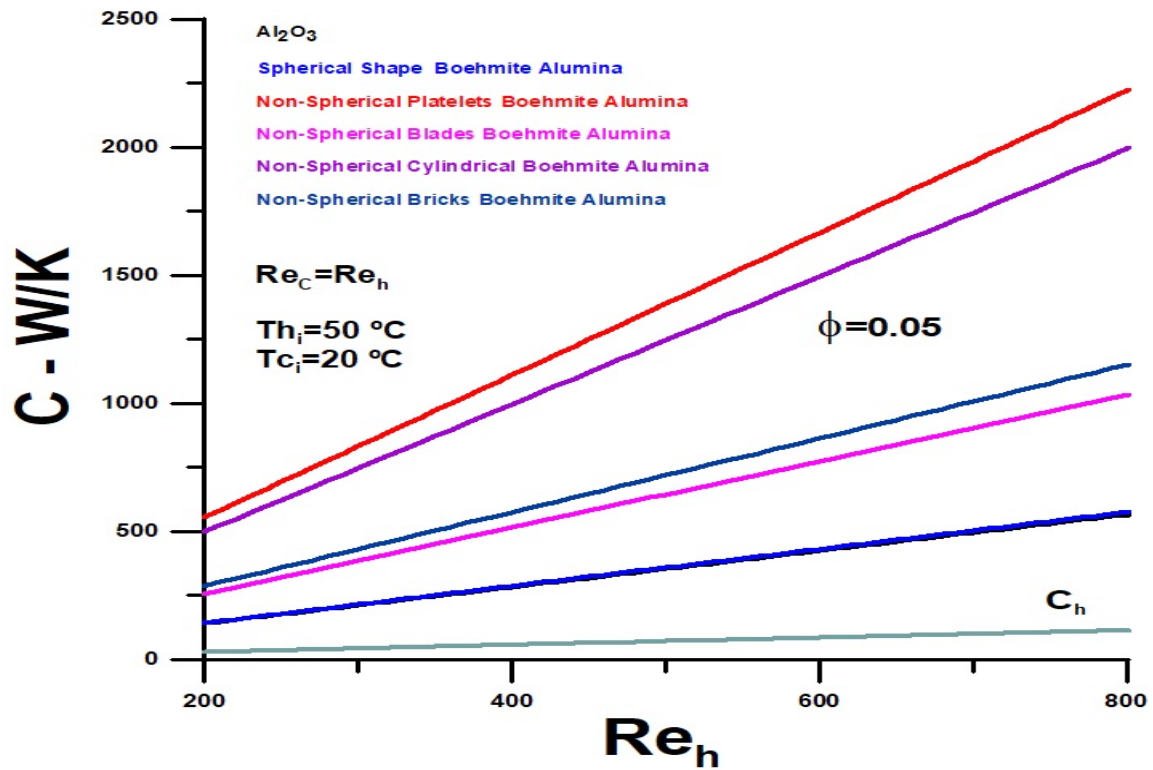

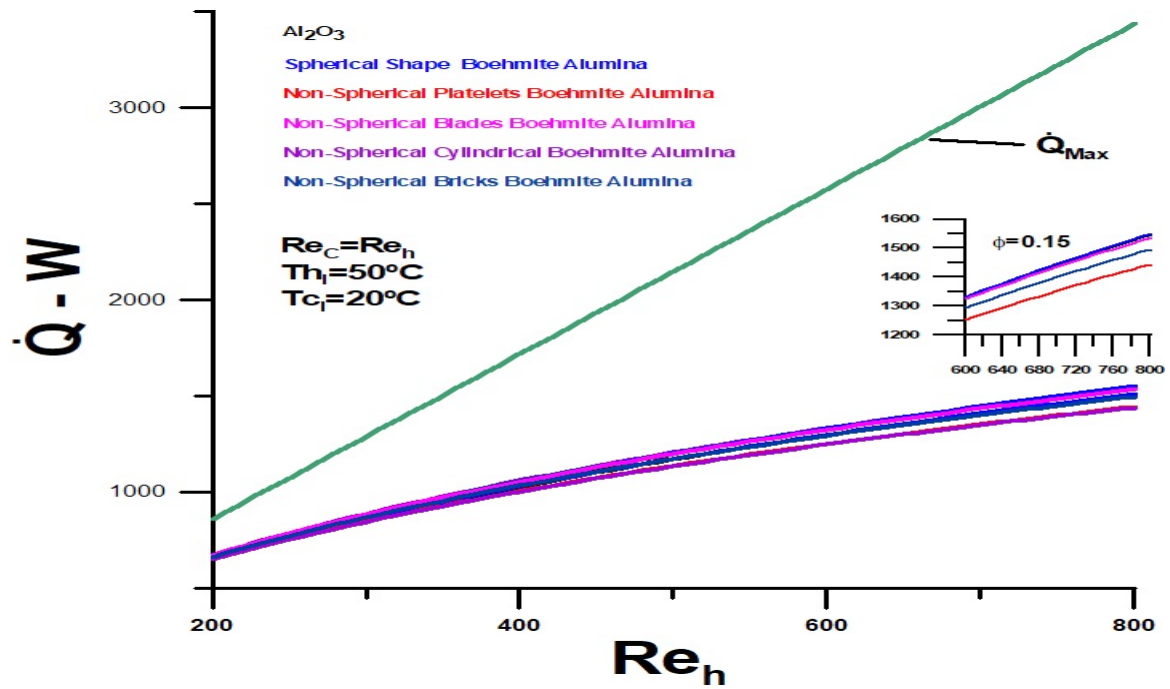**Figure 5.** Thermal capacity versus Reynolds number

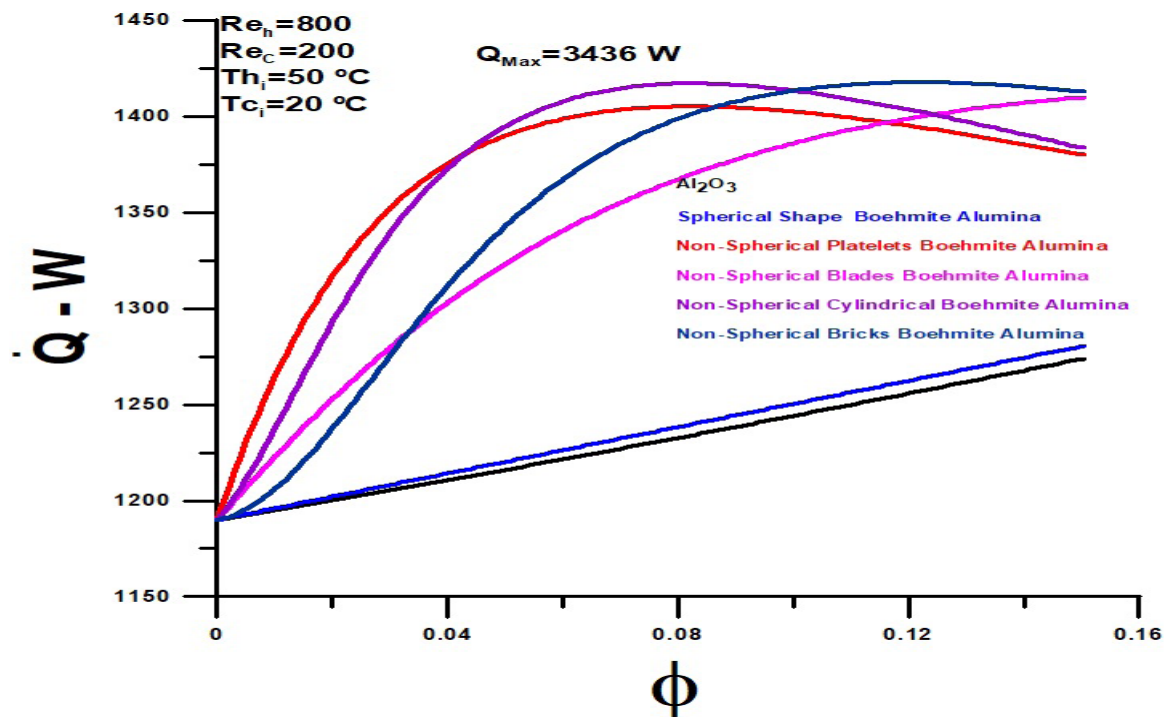**Figure 6.** Actual and maximum heat transfer rate versus Reynolds number

Figure 7. Heat transfer rate versus volume fraction of nanoparticles Re_h=800 and Re_c=200

Figure 8 shows the heat transfer rate as a function of the Prandtl number. The highlighted figure presents Prandtl number versus volume fraction. The Prandtl number grows with the volume fraction similar to that obtained for the momentum diffusivity, and the highest values are obtained for the non-spherical cylindrical and platelet shapes in the entire volume fraction range. The relevant fact is that Prandtl decreases with the increase in volume fraction for the spherical nanoparticles. The central figure, heat transfer rate versus Prandtl, highlights this fact, demonstrating that the Prandtl number increases, the heat transfer rate decreases for spherical nanoparticles, which have relatively low values for the Prandtl number. The highest Prandtl number values are obtained for non-spherical cylindrical and platelet nanoparticles, which have a slightly lower thermal performance than non-spherical blade and Brick type nanoparticles. Non-spherical particles have high values for heat transfer rates regarding spherical particles. It is noteworthy that the heat transfer rate goes through a maximum value with an increase in the Prandtl number, with the rise in the fraction in volume. Non-spherical Blade nanoparticles did not reach the maximum value for heat transfer for the maximum volume fraction under analysis equal to $\Phi=0.15$, and, in this case, it is possible to increase the volume fraction until the maximum heat transfer rate.

Figure 9 presents thermal irreversibility results, representing the generation of entropy, as a function of the volume fraction of the nanoparticles for $Re_h=800$ and $Re_c=200$. Values for thermal irreversibility are relatively low concerning total entropy, which considers the portion of entropy generation associated with the viscosity of the medium. Entropy generation grows with the volume fraction for all nanoparticles and is relatively high for non-spherical nanoparticles compared to entropy generation for spherical particles. The nanoparticle shapes affect the interaction between the base fluid and the nanoparticles, creating greater irreversibility. There is a clear relationship between the heat transfer rate exchanged between fluids and irreversibility (Figure 7). The greater irreversibility is achieved for non-spherical cylindrical and platelet nanoparticles. The entropy generation rate did not reach the maximum for the non-spherical nanoparticle Blade, within the volume fraction range equal to 0.0 and 0.15. The maximum entropy generation for the non-spherical nanoparticle Bricks is reached near the equal volume fraction to 0.15.

Figure 10 presents results for thermal efficiency as a function of the volume fraction of the nanoparticles for $Re_h=800$ and $Re_c=200$. Efficiency is low where irreversibility is high, when heat transfer rate is high, or when there is high entropy generation. In this sense, Figures 8
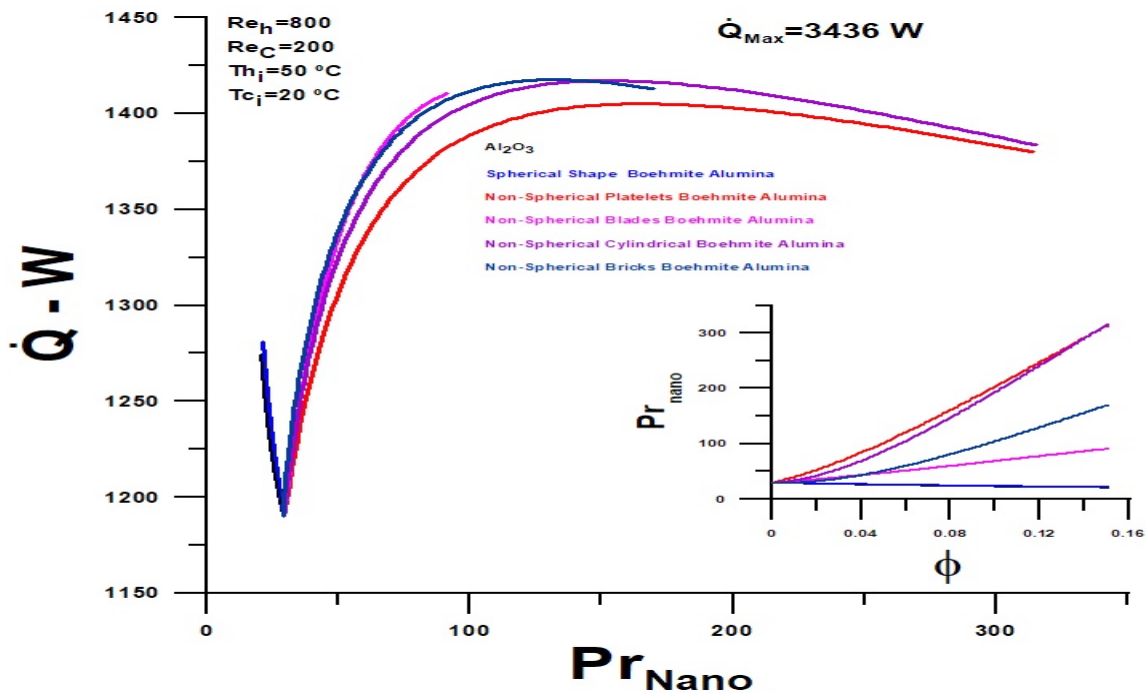

Figure 8. Heat transfer rate versus Prandtl number and Prandtl number versus volume fraction $Re_h=800$ and $Re_c=200$
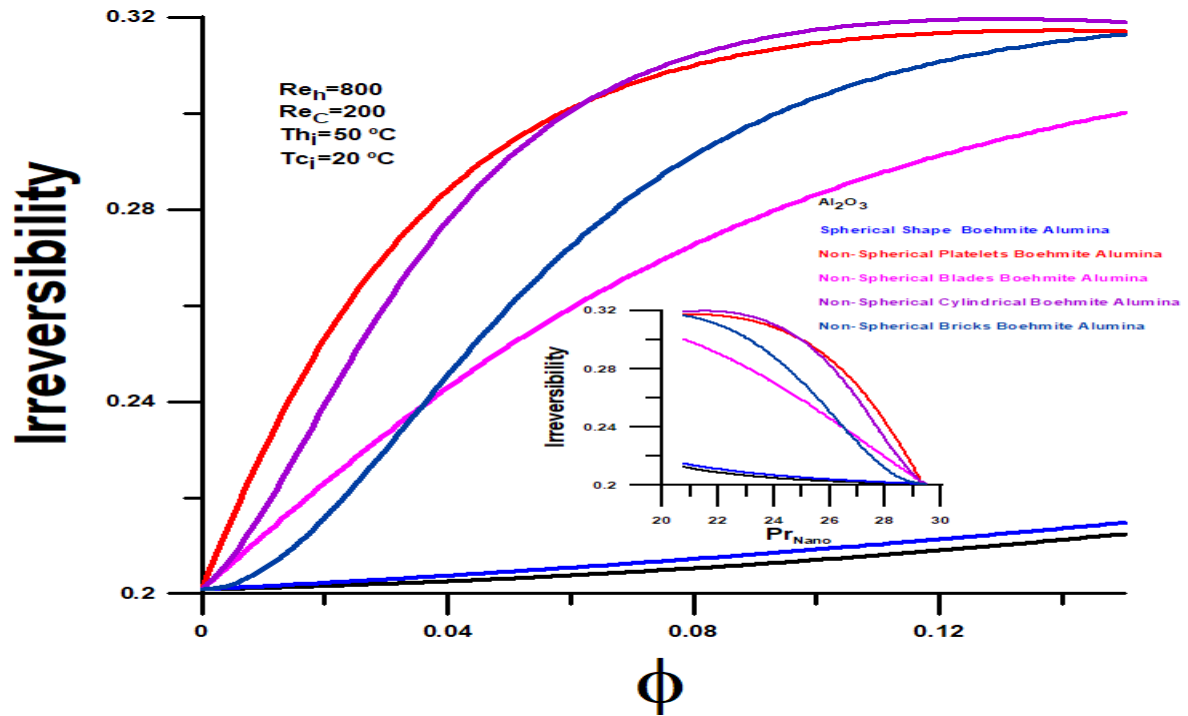
Figure 9. Irreversibility versus volume fraction of nanoparticles and Prandtl number Re_h=800 and Re_c=200
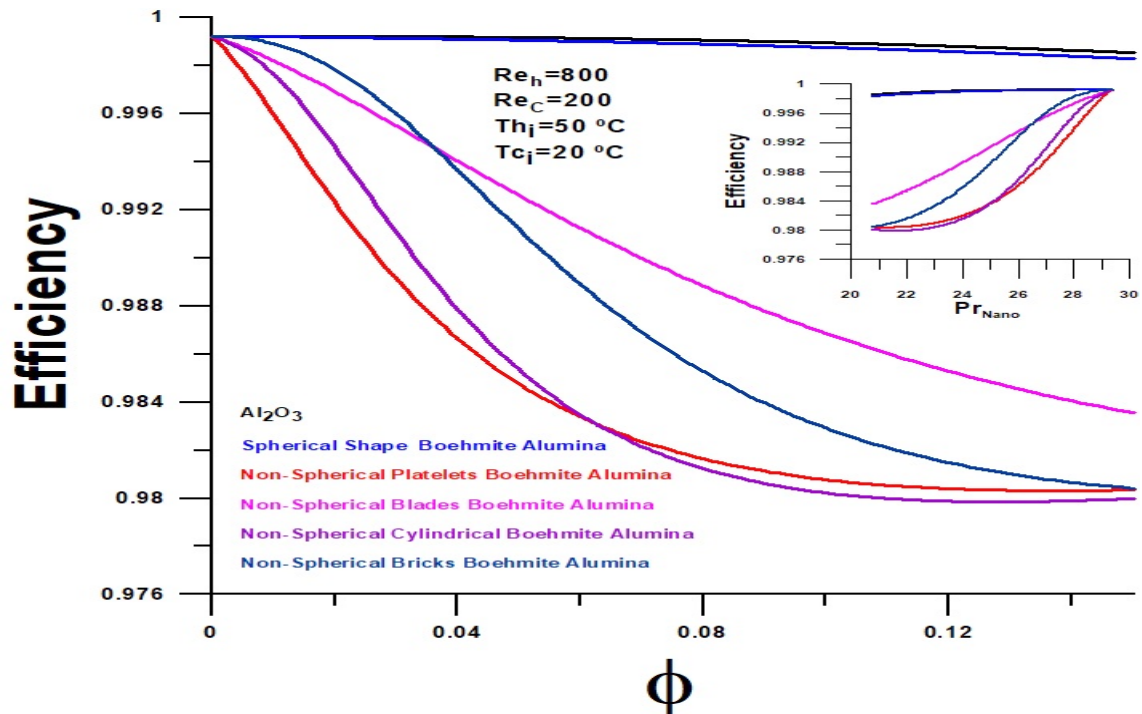

Figure 10. Efficiency versus volume fraction of nanoparticles and Prandtl number Re_h=800 and Re_c=200

and 9 complements each other and corroborate the results obtained for the heat transfer rate observed for the nanofluid through Figures 6 and 7.

Figure 11 shows the hot fluid outlet temperature as a function of the volume fraction of the nanoparticles and complements the information already obtained for Re_h=800 and Re_c=200. The lowest outlet temperature occurs when irreversibility is high or greater heat exchange between the media, corresponding to non-spherical cylindrical and brick nanoparticles for different volume fractions. Cylindrical nanoparticles reach a lower temperature in a volume fraction equal to 0.8 and the brick nanoparticle close to 0.12. For blade nanoparticles, a lower output temperature can be reached for a volume fraction greater than 0.15.

Figure 12 presents results of heat transfer rate versus volume fraction for the nanoparticles, with Re_h=800 and Re_c=600 as parameters. The absolute values of the heat transfer rate are significantly higher concerning the condition Re_h=800 and Re_c=200. For smaller volume fractions of nanoparticles, platelets and cylindrical particles increase the heat transfer rate and higher value. In these cases, when the volume fraction increases, they go through a maximum heat transfer rate between 0.4 and 0.8 and decrease until the heat transfer rate is below the value obtained for the spherical nanoparticles for volume fractions above 0.10. For volume fractions above 0.8, Blades and Bricks nanoparticles show better thermal performance than others. The non-spherical blade nanoparticle has a higher heat transfer rate than spherical nanoparticles in the entire range of analyzed volume fraction.

Figure 13 shows heat transfer rate versus Prandtl number, and highlighted figure presents Prandtl number versus volume fraction, for Re_h= 800 and Re_c=600. The Prandtl number decreases with increasing volume fraction for spherical nanoparticles. Heat transfer rate versus Prandtl demonstrates that when the Prandtl number rises, the heat transfer rate decreases for spherical nanoparticles, which have relatively low values for the Prandtl number. The highest Prandtl number values are obtained for cylindrical and non-spherical platelet nanoparticles, with slightly lower thermal performance than the non-spherical blade and Brick-type nanoparticles. Non-spherical particles have high values for heat transfer rates relative to spherical particles. The heat transfer rate goes through a maximum value as the Prandtl number increases, that is, as the volume fraction increases for all non-spherical nanoparticles. All non-spherical nanoparticles have a maximum value for the heat transfer rate for a volume fraction between 0.4 to 0.6, with nanoparticle bricks with a higher absolute value. Platelets and cylindrical nanoparticles have lower heat transfer rates than those obtained for spherical nanoparticles for high volume fractions.

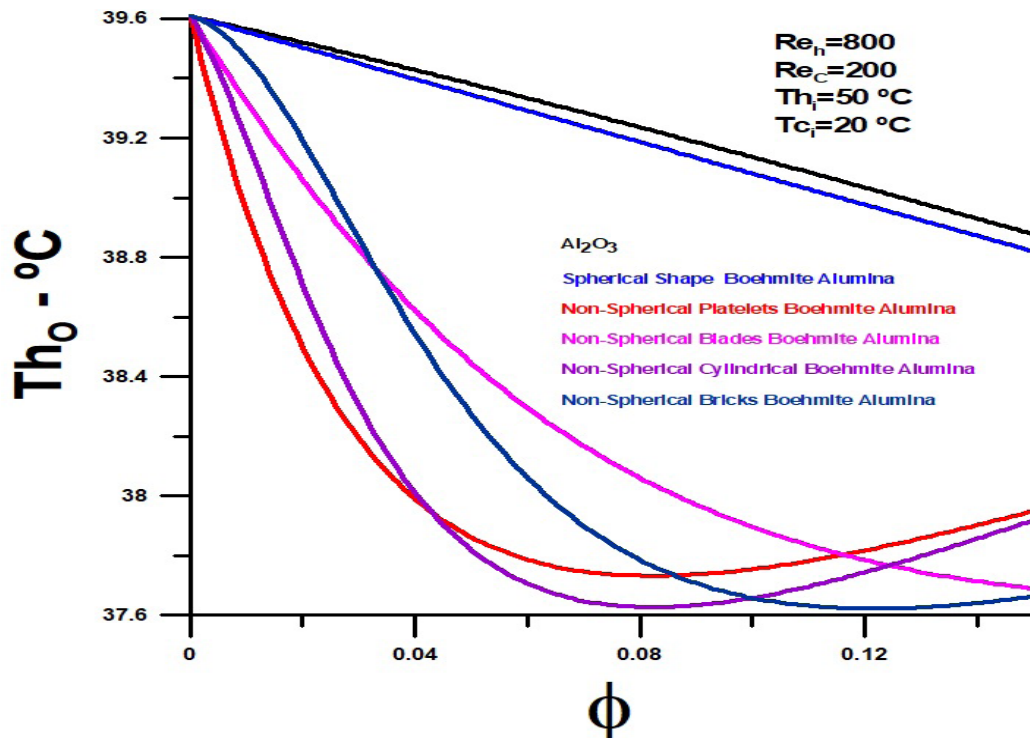Figure 14 presents thermal irreversibility results, rep-

Figure 11. Fluid hot exit temperature versus volume fraction of nanoparticles number Re_h=800 and Re_c=200
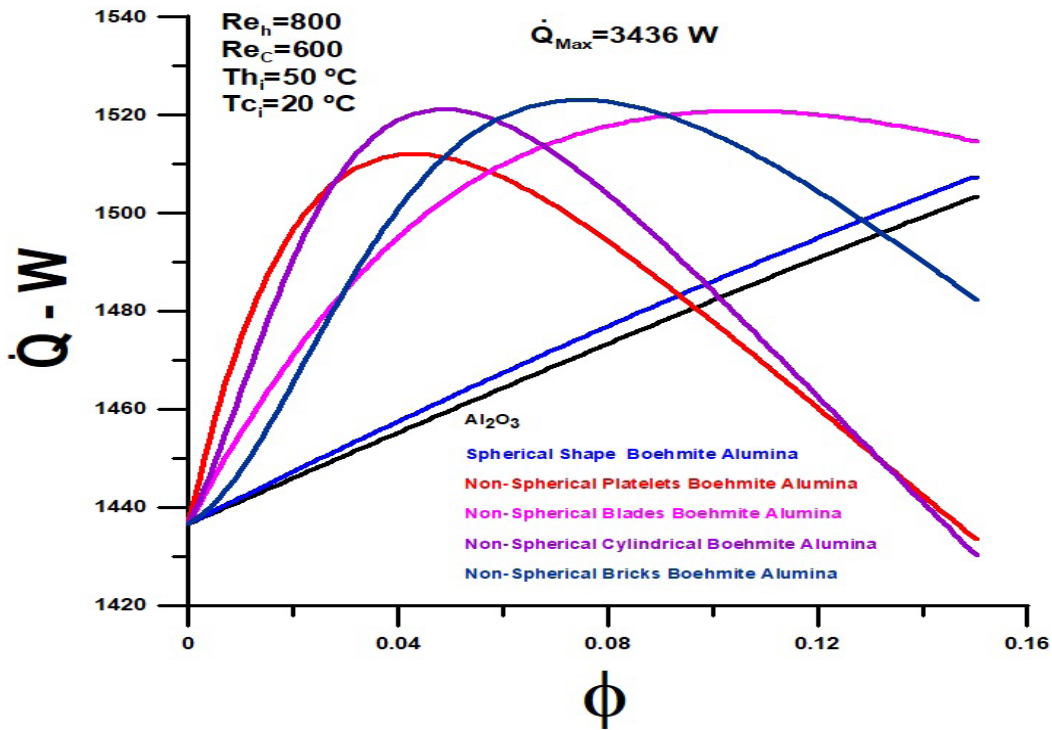
Figure 12. Heat transfer rate versus volume fraction of nanoparticles Re_h=800 and Re_c=600

resenting the generation of entropy, as a function of the volume fraction of the nanoparticles for Re_h=800 and Re_c=600. Values for thermal irreversibility are relatively low concerning total entropy, which considers the portion of entropy generation associated with the viscosity of the medium. Entropy generation grows with the volume fraction for all nanoparticles and is relatively high for non-spherical nanoparticles compared to entropy generation for spherical particles. The results, in this case, show numerical values more elevated than the situation already analyzed, Re_h=800 and Re_c=200, and reflect the higher heat transfer rate. The nanoparticle shapes affect the interaction between the fluid base and the nanoparticles. Greater irreversibility is achieved for non-spherical cylindrical and platelet nanoparticles for volume fraction small and medium values. The entropy generation rate did not reach the maximum for the non-spherical nanoparticles blade and brick, within the volume fraction range equal to 0.0 and 0.15. The maximum entropy generation for these non-spherical nanoparticles is reached at a volume fraction equal to 0.15.

Figure 15 presents results for thermal efficiency as a function of the volume fraction of the nanoparticles for Re_h=800 and Re_c=600. Efficiency is low where irreversibility is high, when heat transfer rate is high, or when there is high entropy generation.

Figure 16 shows the hot fluid outlet temperature as a function of the volume fraction of the nanoparticles and complements the information already obtained for Re_h=800 and Re_c=600. The hot fluid outlet temperatures are always lower than Re_h=800 and Re_c=200. The lowest outlet temperature occurs when irreversibility is high or greater heat exchange between the media, corresponding to non-spherical cylindrical and brick nanoparticles for volume fractions between 0.4 to 0.6. For blade and nanoparticles bricks, lower output temperature can be reached for a volume fraction between 0.6 to 0.15. The relevant fact is that the hot fluid exit temperature may be lower for spherical nanoparticles for high volume fractions.

Figures 17 and 18 present the hot fluid exit temperature values of the two different volume fractions. For a volume fraction equal to 0.05, the exit temperatures for non-spherical nanoparticles are, in all cases, lower than the exit temperatures for spherical nanoparticles. As already observed, for a fraction in a volume equal to 0.15, the only nanoparticle that present exit temperatures lower than those obtained for spherical nanoparticles are those that have the shape of the blade. The lowest exit temperatures for all nanoparticles are obtained for Re_h=200 and Re_c=200.

In summary, the results highlight platelets and cylindrical nanoparticles for Reynolds numbers Re_h=800 and Re_c=200 and demonstrate a higher heat transfer rate for low volume fractions. On the other hand, the brick and
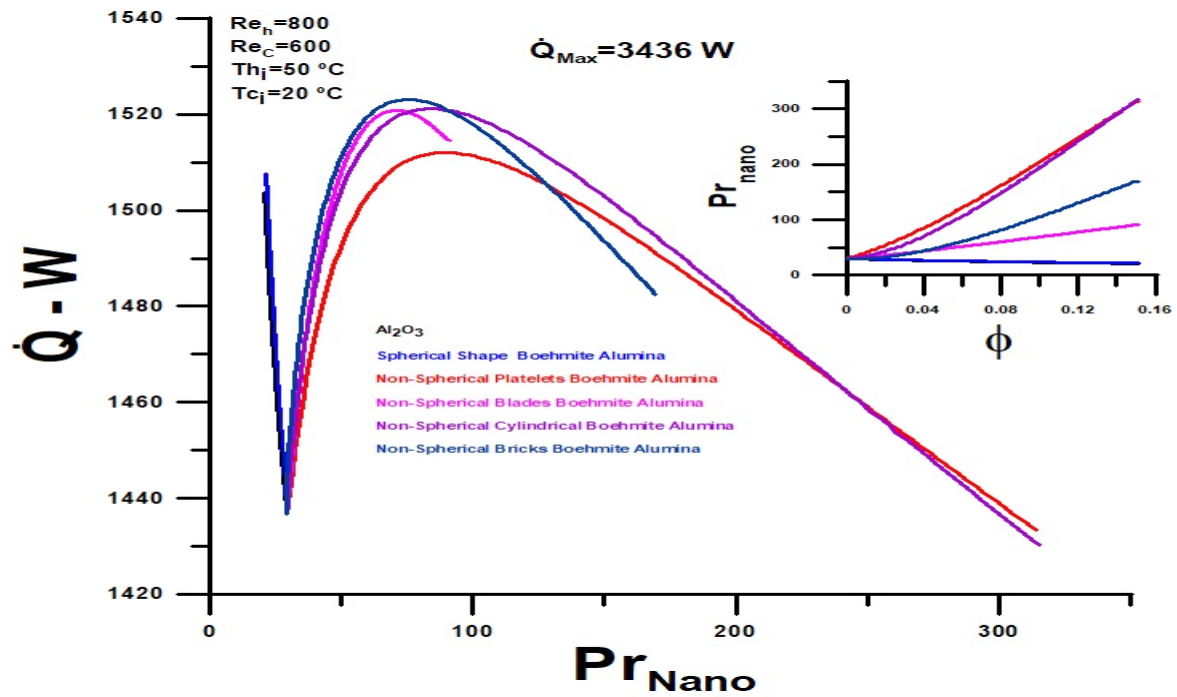
Figure 13. Heat transfer rate versus Prandtl number and Prandtl number versus volume fraction $Re_h=800$ and $Re_c=600$
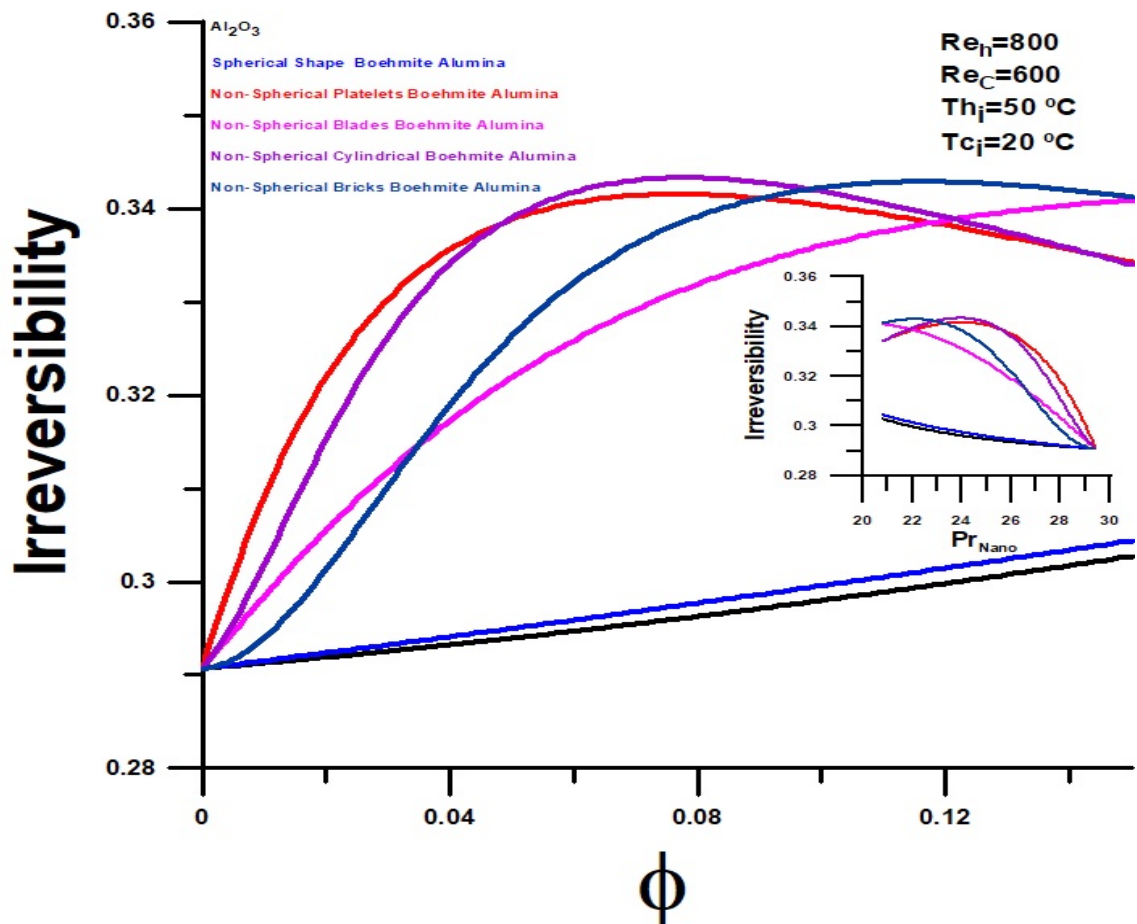

Figure 14. Irreversibility versus volume fraction of nanoparticles and Prandtl number $Re_h=800$ and $Re_c=600$
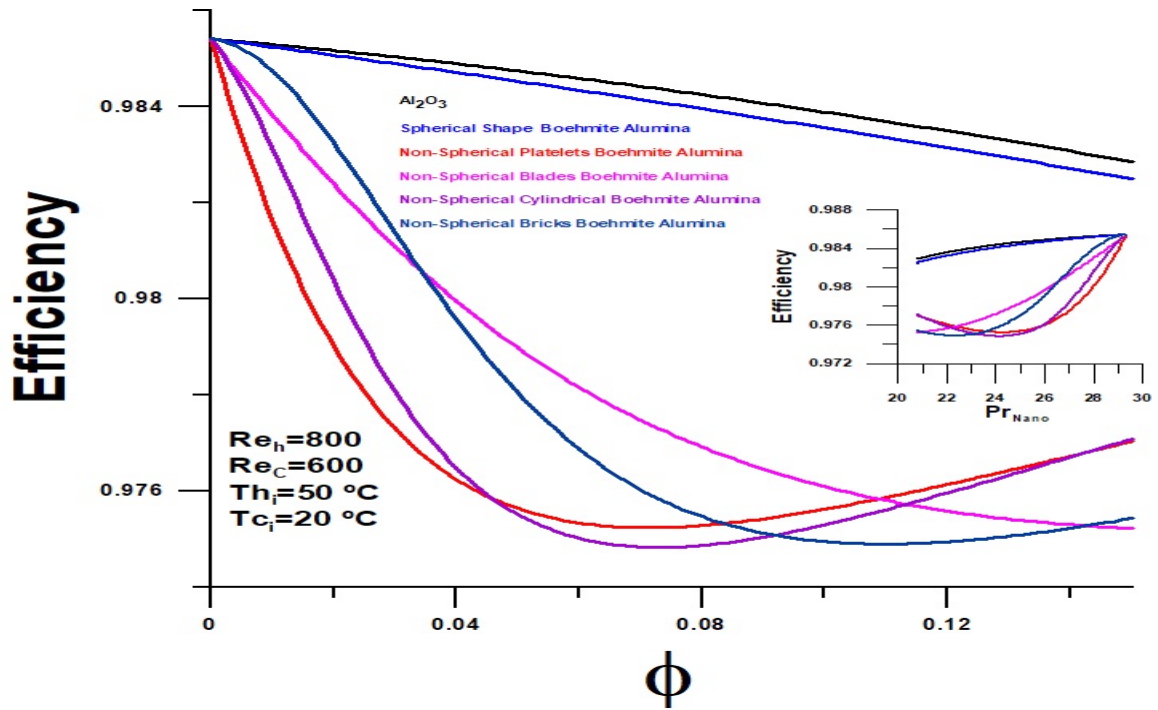
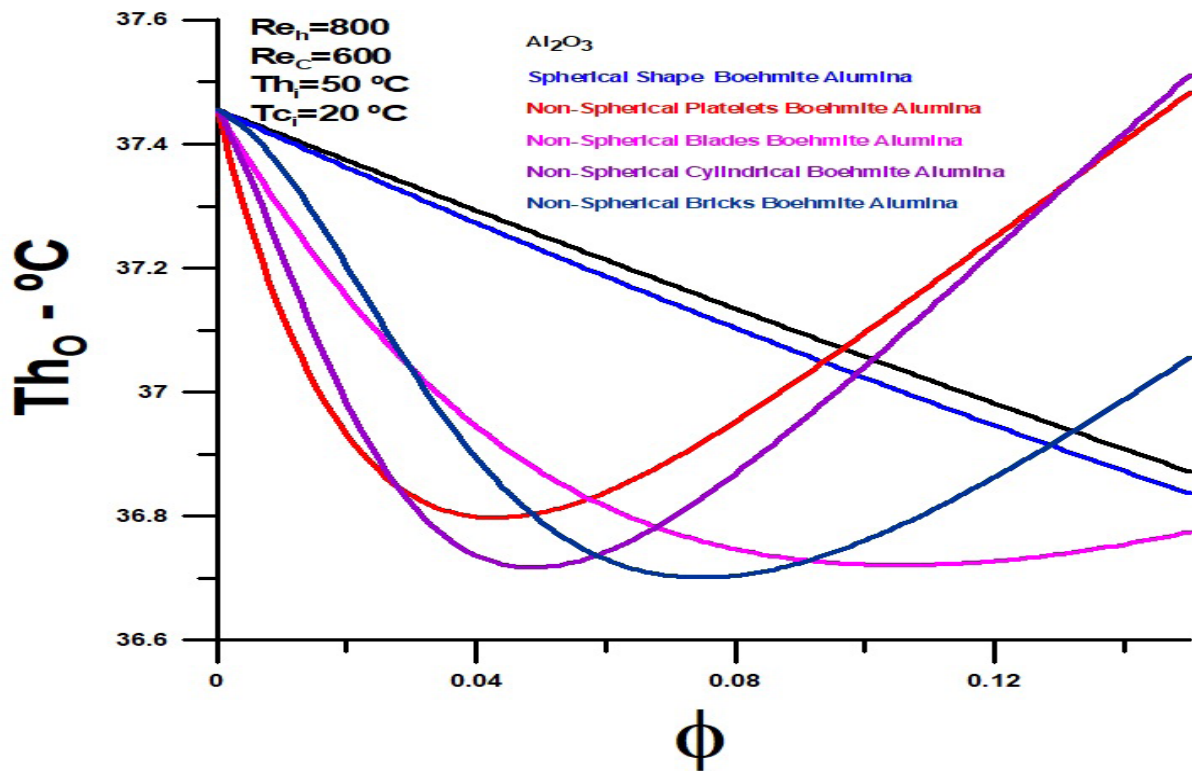**Figure 15.** Efficiency versus volume fraction of nanoparticles and Prandtl number Re_h=800 and Re_c=600

Figure 16. Fluid hot exit temperature versus volume fraction of nanoparticles Re_h=800 and Re_c=600
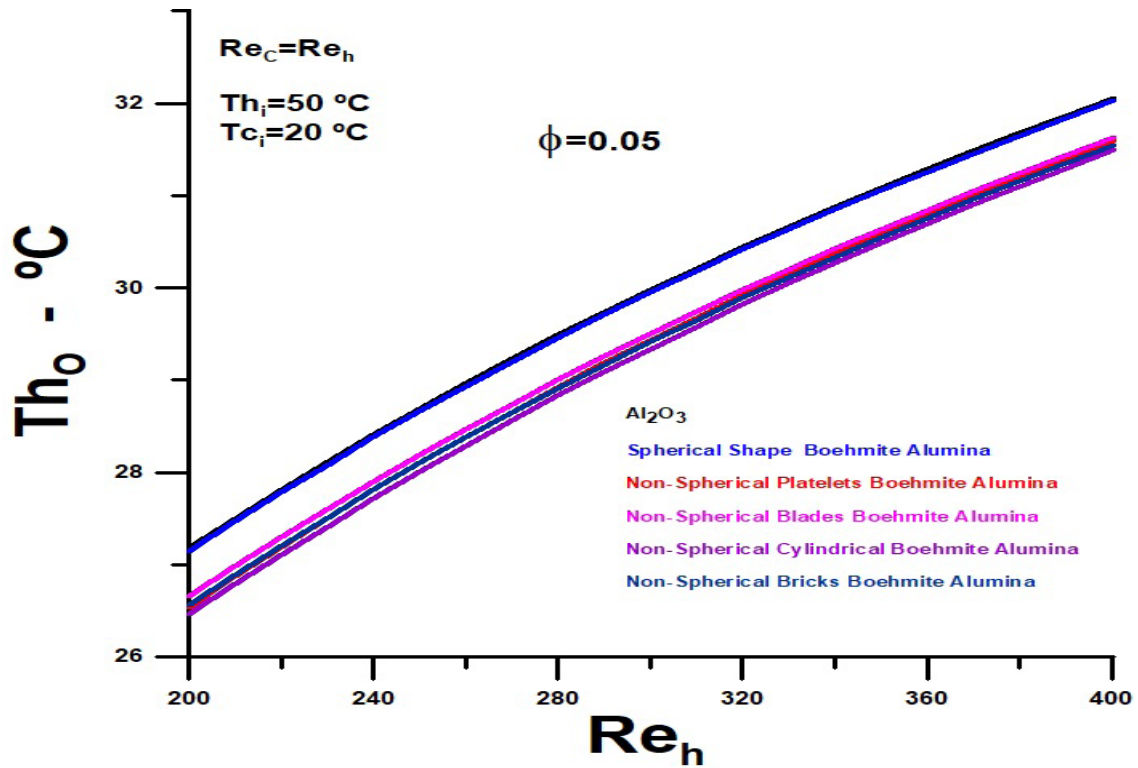
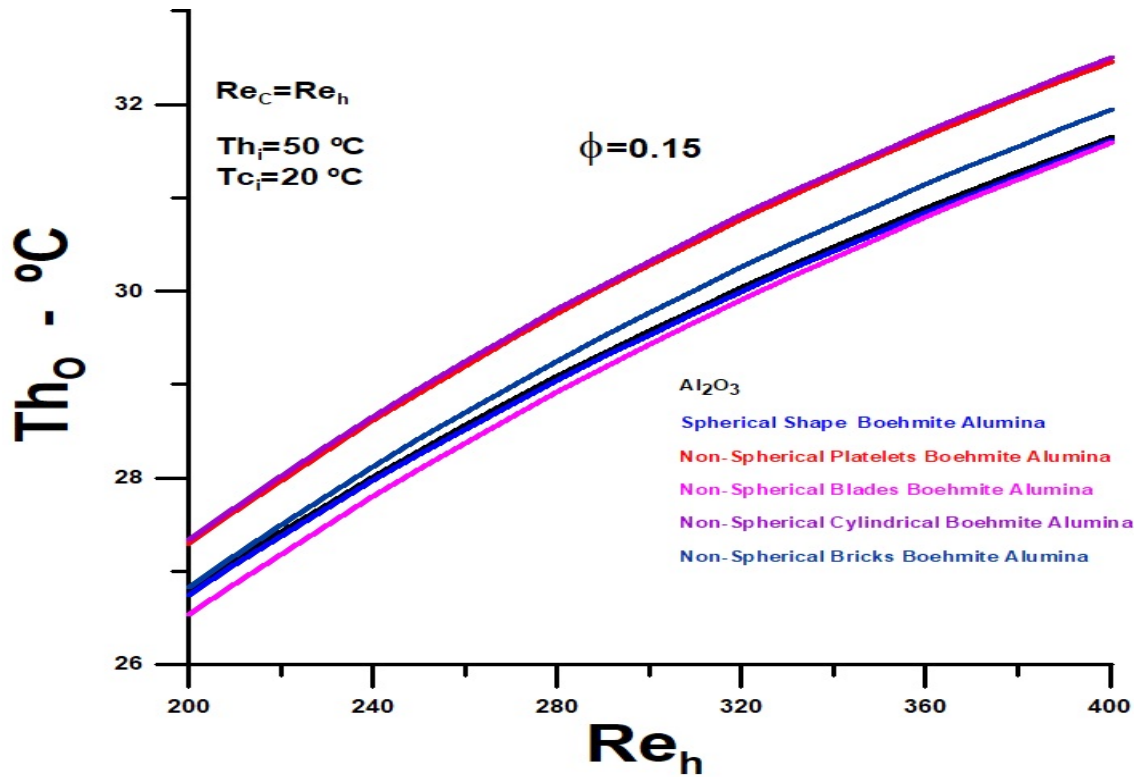**Figure 17.** Fluid hot exit temperature versus Reynolds number for Φ=0.05

Figure 18. Fluid hot exit temperature versus Reynolds number for Φ=0.15

blade-shaped particles outperform the previous two for high volume fraction values. The non-spherical blade nanoparticle does not reach the maximum heat transfer value for the higher volume fraction under analysis equal to Φ = 0.15.

For Reynolds numbers, Re_h=800 and Re_c=600 brick and blade nanoparticles have better thermal performance for volume fraction above 0.8, and non-spherical blade nanoparticle has a higher heat transfer rate than spherical nanoparticles across the entire volume fraction range analyzed. For a volume fraction above 0.10, platelets and cylindrical particles present the transfer rate below the value obtained for spherical nanoparticles. The lowest hot fluid exit temperature for brick and blade nanoparticles occurs for volume fractions between 0.6 to 0.15. Still, the hot fluid exit temperatures are always lower than Reh=800 and Rec=200 conditions.

4. Conclusions

The thermal performance of a printed circuit heat exchanger (PCHE) was determined using non-spherical nanoparticles compared to spherical nanoparticles. The analysis covered Reynolds values equal to 200 and 800 for the hot fluid and 200 and 600 for cold fluid, with volume fractions for the nanoparticles ranging from 0.05 to 0.15. The spherical particles are Al_2O_3 and Boehmite alumina, and the non-spherical particles of Boehmite alumina are platelets, blades, cylindrical, and bricks.

It was demonstrated that non-spherical particles have higher heat transfer rates than spherical particles. Applying the second law of thermodynamics methodology makes thermal performance analysis straightforward and elegant.

In specific terms, the work highlights:

- The nanoparticles' shapes affect the interaction between the fluid base and the nanoparticles, creating greater thermal irreversibility.

- Thermal entropy generation grows with the volume fraction for all nanoparticles and is relatively high for non-spherical nanoparticles than thermal entropy generation for spherical particles.

- The maximum theoretically possible heat transfer rate is associated with the hot fluid and serves as a reference for current heat transfer rates.

- Spherical nanoparticles present very close graphic results, as they have similar numerical thermodynamic properties.

- For volume fraction equal to 0.05, the hot fluid exit temperatures for non-spherical nanoparticles are in all cases lower than the hot exit temperatures for spherical nanoparticles.

- For a volume fraction equal to 0.15, the only nanoparticles that present lower hot fluid exit temperatures than those obtained for spherical nanoparticles are those that have the shape of a blade.

- For all nanoparticles under analysis, the lowest hot fluid exit temperatures are obtained for Re_h=200 and Re_c=200.

Conflict of Interest

The Author(s) declare(s) that there is no conflict of interest.

References

[1] Bejan, A., 1987. The thermodynamic design of heat and mass transfer processes and devices. Heat and Fluid Flow. 8(4), 258-276.

[2] Fakheri, A., 2007. Heat Exchanger Efficiency. Transactions of the ASME. 129, 1268-1276.
DOI: http://dx.doi.org/10.1016/j.applthermaleng.2017.05.076

[3] Tiwari, R., Maheshwari, G., 2017. Effectiveness and efficiency analysis of parallel flow and counter flow heat exchangers. IJAIEM. 6, 314-319.

[4] Nogueira, E., 2020. Thermal performance in heat exchangers by the irreversibility, effectiveness, and efficiency concepts using nanofluids. Journal of Engineering Sciences. 7, F1-F7.
DOI: https://doi.org/10.21272/jes.2020.7(2).f1.

[5] Nogueira, E., 2021. Efficiency and Effectiveness Thermal Analysis of the Shell and Helical Coil Tube Heat Exchanger Used in an Aqueous Solution of Ammonium Nitrate Solubility (ANSOL) with 20% H_2O and 80% AN. Journal of Materials Science and Chemical Engineering. 9, 24-45.
DOI: https://doi.org/10.4236/msce.2021.96003

[6] Chai, L., Tassou, S.A., 2020. A review of printed circuit heat exchangers for helium and supercritical CO_2 Brayton cycles. Thermal Science and Engineering Progress, 18(2020), 100543.
DOI: https://doi.org/10.1016/j.tsep.2020.100543

[7] Seo, J.W., Kim, Y.H., Kim, D., Choi, Y.D., Lee, K.J., 2015. Heat Transfer and Pressure Drop Characteristics in Straight Microchannel of Printed Circuit Heat Exchangers. Entropy. 17, 3438-3457.
DOI: https://doi.org/10.3390/e17053438

[8] Almurtaji, S., Ali, N., Teixeira, J.A., Addali, A., 2020. On the Role of Nanofluids in Thermal-Hydraulic Performance of Heat Exchangers—A Review. Nanomaterials. 10, 734.
DOI: https://doi.org/10.3390/nano10040734.

[9] Zahmakesh, I., Sheremet, M., Y., Heris, S.Z., Mohsen, S., Josua, P., Meyere, M.G., Wongwises, S., Jingj, D., Mahiankl, O., 2021. Effect of nanoparticle shape on the performance of thermal systems utilizing nanofluids: A critical review. Journal of Molecular Liquids. 321(1), 114430.

DOI: https://doi.org/10.1016/j.molliq.2020.114430

[10] Monfared, M., Shahsavar, A., Bahrebar, M.R., 2019. Second law analysis of turbulent convection flow of boehmite alumina nanofluid inside a double-pipe heat exchanger considering various shapes for nanoparticle. Journal of Thermal Analysis and Calorimetry. 135, 1521-1532.

DOI: https://doi.org/10.1007/s10973-018-7708-7

[11] Behrouz, R., Peyghambarzadeh, S.M., 2019. Measurement of Local Convective Heat Transfer Coeffi-

cient of Alumina-Water Nanofluids in a Double Tube Heat Exchanger. Journal of Chemical and Petroleum engineering. 53(1), 25-36.

DOI: https://doi.org/10.22059/jchpe.2019.265521.1247

[12] Elena, V., Timofeeva, J., Routbort, L., Dileep, S., 2009. Particle shape effects on thermophysical properties of alumina nanofluids. Journal of Applied Physics. 106, 014304.

DOI: https://doi.org/10.1063/1.3155999

[13] Zhou, X.F., 2006. Effective thermal conductivity in nanofluids of non-spherical particles with interfacial thermal resistance: Differential effective medium theory. Journal of Applied Physics. 100, 024913.

DOI: https://doi.org/10.1063/1.2216874

[14] Kays, W.M., London, A.L., 1984. Compact Heat Exchangers. MacGraw-Hill, New York.